Transactions, SMiRT-23
Manchester, United Kingdom - August 10-14, 2015
Division 1, Paper ID 640, Mechanics of Materials

THE EFFECT OF IRRADIATION TEMPERATURE ON PRECIPITATION IN RPV STEELS

Sarah Connolly[1], Jonathan Hyde[2], Philippe Pareige[3], David Parfitt[4], Paul Styman[5] and Keith Wilford[6]

[1] D.Phil Student, Department of Materials, University of Oxford, UK
[2] Chief Technologist, National Nuclear Laboratory, UK & Department of Materials, University of Oxford, UK
[3]Director, Rouen University, CNRS, INSA Rouen, France
[4] Materials Specialist, Rolls-Royce, Derby, UK
[5] Graduate Scientist, National Nuclear Laboratory, UK
[6] Materials Specialist, Rolls-Royce, Derby, UK

ABSTRACT

The Reactor Pressure Vessel (RPV) is one of the most important components for the safety of nuclear power plants. The safety goal is to avoid catastrophic failure of the RPV and this can only be achieved using a structural integrity evaluation based on fracture mechanics to ensure sufficient margin against failure during transients. RPV embrittlement has been an issue for over 50 years but it is only in the last 20 years or so that dramatic improvements in microstructural techniques have enabled development of mechanistic insight that can be used to underpin predictions of properties of the RPV during service.

Microstructural observations obtained from Atom Probe Tomography (APT) have proved immensely valuable. For instance the development of 2nm diameter solute clusters has been directly linked to changes in hardness and hence embrittlement of RPV steels. In this work APT has been used to study the irradiation response of several low and high Ni RPV test welds irradiated at temperatures between 220°C and 310°C. The extent of irradiation-induced clustering correlated with bulk Cu levels and evidence was found supporting more rapid development of solute clusters at higher irradiation temperatures. At lower irradiation temperatures the contribution from matrix damage to the irradiation hardening response increased and the solute clusters were found to be more enriched in Si. Overall the general trend of increasing hardness with cluster volume fraction was confirmed.

INTRODUCTION

The integrity of the RPV is one of the most important issues affecting the safe and economic operation of commercial Light Water Reactor (LWR) Nuclear Plants [1]. This is because the RPV, as well as providing the primary containment pressure boundary also provides the principal containment of the core components. PWR vessels typically experience pressures of ~15MPa and temperatures of ~290°C during normal steady state operation whereas BWR vessels typically operate at lower temperatures (~270°C) and pressures (~7MPa). Current RPVs are made from various grades of ferritic steels. These materials exhibit a ductile to brittle transition (DBT) as the temperature is decreased. Furthermore, during service the material properties degrade and the DBT temperature (DBTT) decreases. Safe operation is determined by P-T limits which requires plants to operate above a certain minimum temperature (T) and below a maximum pressure (P).

The degradation of material properties results from irradiation damage at the atomic scale. Point defects are formed by the interaction between incident fission neutrons and the lattice atoms. The subsequent microstructural development depends both on the migration and clustering of the point defects produced and on a complex interaction of these point defects with solute atoms. The resulting microstructure is often observed to contain a range of microstructural features. These can include a high density of ~2nm solute clusters as well as matrix damage (e.g. dislocation loops, vacancy and interstitial clusters) which impede dislocation movement and cause hardening and embrittlement [2]. It is important to appreciate

that the development of the microstructure will depend on irradiation temperature. The number of point defects present is based on an equilibrium between their rate of creation and their rate of loss through diffusion to fixed sinks and traps. Whilst temperature in the range of interest has little effect on rates of generation, the reduced mobility at lower temperatures results in a net increase in defects present in the matrix.

The most complete analysis, over the widest range of temperature and dose rates, is provided by the early data of Barton et al [3] and Grounes [4] on CMn steels, and analysed by Jones and Williams [5]. Each data set exhibited an irradiation induced increase in tensile yield stress ($\Delta\sigma_y$) that was proportional to the square root of the fluence.

$$\Delta\sigma_y = A\,(\varphi t)_{Ni}^{1/2}$$

in which A is a material- and temperature-dependent coefficient and $(\varphi t)_{Ni}$ is the neutron fluence according to Ni monitors. Jones and Williams analysed the temperature dependence of A for all the Barton and Grounes data and found a linear relationship

$$F_{T(\Delta\sigma)} = 1.869\text{-}4.57\text{x}10^{-3}T$$

where T is the irradiation temperature in °C and $F_{T(\Delta\sigma)} = A_T/A_{190°C}$ (i.e. using a reference temperature of 190°C). The relationship demonstrates an increase in irradiation hardening and embrittlement with decreasing irradiation temperature and is valid for these CMn steels for irradiation temperatures between ~100°C and 300°C. In the absence of non-hardening embrittlement, it is often observed that $\Delta\sigma$ is proportional to ΔT (the shift in the DBTT) [6, 10], hence the temperature dependence also applies to the Charpy transition shift. This ratio ($\Delta\sigma/\Delta T$) is different for differing types of material (welds/plates) [7].

More recent data has demonstrated that the irradiation temperature response is strongly influenced by composition. Data from low Cu RPV steels are generally supportive of the temperature correction factor F_T [8, 9, 10] and cover a much broader range of steels including MnMoNi steels with low (<0.3wt.%), medium (0.6-0.9wt.%) and high (>3wt.%) levels of Ni. Analyses of data from high Cu RPV steels are more complex because the temperature dependence of embrittlement is affected by both composition and flux, thus the extraction of a discrete temperature term from surveillance databases in which temperature and flux are confounded is difficult. Nonetheless, the general trend of increasing embrittlement with decreasing irradiation temperature remains clear.

Microstructural techniques, such as Small Angle Neutron Scattering (SANS), Transmission Electron Microscopy (TEM) and Atom Probe Tomography (APT) [11], can now be used to help develop a mechanistic understanding for this temperature dependence. For instance Meslin et al [12] reported that increasing the irradiation temperature between 200°C and 400°C increased the diameter and decreased the number density of interstitial dislocation loops in ion-irradiated Fe-40ppm C. Watanabe used TEM techniques to examine the formation of dislocation loops induced by electron irradiations at different temperatures [13]. The loop concentration increased with decreasing irradiation temperatures in pure Fe and Fe-Mn model alloys but the temperature dependence was weak in an A533B steel (JRQ).

Jones and Bolton [14] reviewed solute cluster size data from a large number of alloys and steels irradiated at surveillance and accelerated rates at temperatures between 150°C and 400°C and found that the mean cluster sizes were relatively insensitive to irradiation temperatures below ~300°C but at higher temperatures cluster coarsening occurs. Odette and co-workers [15] used SANS to study the effect of irradiation temperature on MnMoNi steels and related model alloys in the range 270°C – 310°C (the IVAR program). Separation of the data according to constant flux, fluence and Cu content, demonstrated that solute cluster coarsening occurs with increasing irradiation temperature even between 270°C and 310°C. Furthermore some evidence for increasing cluster number density with decreasing irradiation temperature was observed.

Further microstructural data is needed to improve our understanding of the effect of irradiation temperature on the embrittlement of RPV steels. In this work APT has been used to study the irradiation response of several low and high Ni RPV test welds irradiated at temperatures between 220°C and 310°C.

MATERIALS AND EXPERIMENTAL CONDITIONS

Table 1 details the compositions and irradiation conditions of the RPV test welds selected for study. The welds were annealed at 920°C for 6 hours and then water quenched, tempered at 600°C for 42 hours, given stress relief at 650°C for 6 hours and finally slow cooled. The samples cover a range of Ni and Cu contents. Samples SH (high Cu) and SL (low Cu) both contain low Ni. Samples WV (high Cu) and 2W (lower Cu) both contain high Ni. The range of compositions for C, Si, Mn, Mo and Cr are low in comparison to those for Cu and Ni. The samples were irradiated at temperatures between 225 and 310°C to doses between 8 and 32 mpda at an accelerated rate in a Materials Test Reactor. Vickers hardness tests were performed on each sample using a 20kg load. The irradiation induced increases in hardness are also detailed in Table 1.

Table 1. Nominal compositions of test weld samples (at%). Balance Fe.

Sample	C	Si	Mn	Mo	Ni	Cr	Cu	Irradiation Temp (°C)	Dose (mpda)	Dose Rate (dpa/s)	Change in Hardness (ΔHv)
SH 061	0.24	0.72	1.53	0.27	0.09	0.04	0.45	255	8.3	$6x10^{-9}$	54
SH 511	0.23	0.77	1.51	0.28	0.06	0.04	0.52	310	8.7	$6x10^{-9}$	44
SH 553	0.23	0.77	1.51	0.28	0.06	0.04	0.52	255	16	$6x10^{-9}$	67
SL 092	0.29	0.87	1.65	0.28	0.09	0.04	0.10	290	32	$6x10^{-9}$	26
2W2.220	0.25	0.81	1.54	0.20	1.50	0.12	0.20	225	16	$6x10^{-9}$	62
2W2.276	0.25	0.81	1.54	0.20	1.50	0.12	0.20	310	12.3	$8x10^{-9}$	35
WV 013	0.19	0.75	1.38	0.24	1.63	0.05	0.54	225	24.4	$6x10^{-9}$	99
WV 388	0.19	0.75	1.38	0.24	1.60	0.05	0.47	310	17.4	$6x10^{-9}$	89

APT was performed on each sample at the University of Rouen using the Tomographic Atom Probe (TAP) which has a detection efficiency of 50-60%[16]. Final electropolishing of the samples was performed using 2% perchloric acid in 2-butyoxyethanol to produce atom probe needles with an end radius of 50-100nm. During analysis the tip temperature was maintained at ~50K and a pulse fraction of 20% was used which provides a good balance for minimising the preferential evaporation of Cu atoms whilst not increasing significantly the probability of sample fracture [17]. Despite this, for several of the samples, it was necessary to perform several analyses to obtain sufficient high quality data for analysis. Typically it was possible to analyse regions at least $15x15x100nm^3$. It should be emphasised that the experiments were performed in ~2005 and therefore the volumes analysed, and quality of data obtained, are representative of what was then possible.

Analysis of the data obtained involved several stages. Initially a mass spectrum was created from the mass-to-charge ratio data and each peak identified. The peak at 29.0 atomic mass units results from a combination of $^{58}Fe^{2+}$ and $^{58}Ni^{2+}$. The isotopic abundance of ^{58}Fe is only 0.28% and so the Fe contribution to the peak at 29amu could be determined. Similarly the Ni contribution to the 29.0 peak can be determined from known isotopic abundances of Ni and the observations of the other Ni peaks in the mass spectrum. The observed concentrations of each element were compared with the nominal values. Note that no background calculations were performed (background counts will tend to result in an overestimate of the concentrations of minor solutes). Atom maps were then drawn for each solute element. Clear evidence for the clustering of solute atoms was observed in all material conditions. The maximum separation method [18] was used to quantify the extent of solute clustering in terms of cluster compositions, sizes and number densities. The following parameters were used: Core atoms - Cu, Mn, Ni and Si; D_{MAX}=0.4nm; L=0.3nm; E=0.3nm; N_{MIN} = 10 as recommended in [19] for these types of microstructures and a detection efficiency of ~50%. Finally, to ensure avoidance of characterising solute clustering that would occur in a random solid solution, each cluster analysis was repeated on a random

solid solution model (a dataset in which the identities of each atom had been randomly swapped, thus maintaining the same overall composition and density variations as in the original sample).

RESULTS

Overall Compositions

Peaks associated with the major solute elements are clearly visible in the mass spectrum. However interpretation becomes particularly difficult when peaks associated with minor solute atoms are partially obscured by tails of more major peaks. This is clearly evident in Figure 1 where Fe atoms (from the tail of the peak at 28 amu) will be incorrectly identified as Ni and Cu atoms (peaks between ~30 and ~32.5amu). This will result in an overestimation of the Cu and Ni compositions. However, it should be emphasised that the absolute level of noise remains very low and therefore any significant increase in the local composition of the minor solute elements due to solute clustering will be significantly higher than the noise contribution. Thus the noise levels have a minimal impact on the calculations of cluster size, chemistry and number density.

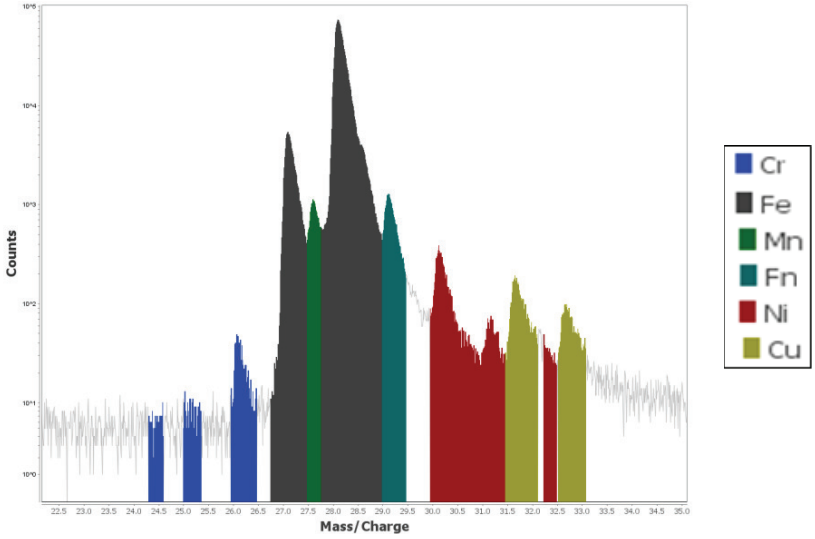

Figure 1. Mass spectrum from WV013 showing that the tail of the Fe peak at 28 amu partially obscures the Ni and Cu peaks. (Fn is a combination of $^{58}Fe^{2+}$ and $^{58}Ni^{2+}$ ions).

Table 2 shows a comparison between the expected composition and the composition found using the TAP, for the main alloying elements. As noted above no background subtraction has been performed. Since background counts have a disproportionate impact on the minor solute elements it might be expected that solute concentrations would have been overestimated. This overestimate is most likely to occur for elements which have several isotopes (e.g. Ni and Mo), are field evaporated in different charge states (e.g. Cu) or where the mass to charge ratios of the ions follow the main Fe^{2+} peak (e.g. Ni and Cu) and indeed this is what is seen – the Ni content has consistently been overestimated. In addition, the observed C, Mn and Mo concentrations tend to be lower than bulk values, and this is due to the presence of carbides and cementite elsewhere.

It can be seen that the mean observed Cu in SH511 is extremely high. This is due to the presence of a large Cu precipitate that will have formed during the post-weld heat treatment. This region was excluded from the analysis volume for all further analyses, so that only irradiation induced solute clustering was characterised.

Table 2. Expected and measured compositions of samples (at%).

Sample	Cu	Mn	Ni	Si	C	Mo	Cr
SL 092 (Nominal)	0.10	1.65	0.09	0.87	0.29	0.28	0.04
SL 092 (Observed)	0.25	1.33	0.57	1.01	0.02	0.28	0.08
SH 061 (Nominal)	0.45	1.53	0.09	0.72	0.24	0.27	0.04
SH 061 (Observed)	0.51	1.37	0.64	0.87	0.02	0.23	0.08
SH 511/553 (Nominal)	0.52	1.51	0.06	0.77	0.23	0.28	0.04
SH 511 (Observed)	2.41	1.28	0.62	0.99	0.03	0.19	0.05
SH 553 (Observed)	0.41	1.24	0.61	0.78	0.01	0.24	0.10
2W2 (Nominal)	0.20	1.54	1.50	0.81	0.25	0.20	0.12
2W2.220 (Observed)	0.24	1.42	1.86	0.85	0.01	0.20	0.12
2W2.276 (Observed)	0.31	1.49	2.48	1.24	0.02	0.17	0.20
WV 388 (Nominal)	0.47	1.38	1.60	0.75	0.19	0.24	0.05
WV 388 (Observed)	0.47	1.31	2.04	0.96	0.02	0.17	0.10
WV 013 (Nominal)	0.54	1.38	1.63	0.75	0.19	0.24	0.05
WV 013 (Observed)	0.44	1.30	2.03	0.86	0.04	0.21	0.07

Analysis of Solute Clusters

Figure 2 shows the distribution of Cu, Mn, Ni and Si atoms observed in WV388. The maximum separation method was used to identify clusters which could then be individually characterised. Figure 3 shows the integrated number density of clusters versus the number of core atoms for WV388 compared with that expected from a random solid solution. The key point to note is that very few clusters containing more than 10 core atoms would be observed in a random solid solution and therefore setting N_{MIN} to 10 was appropriate. Similar checks were made on all of the other datasets.

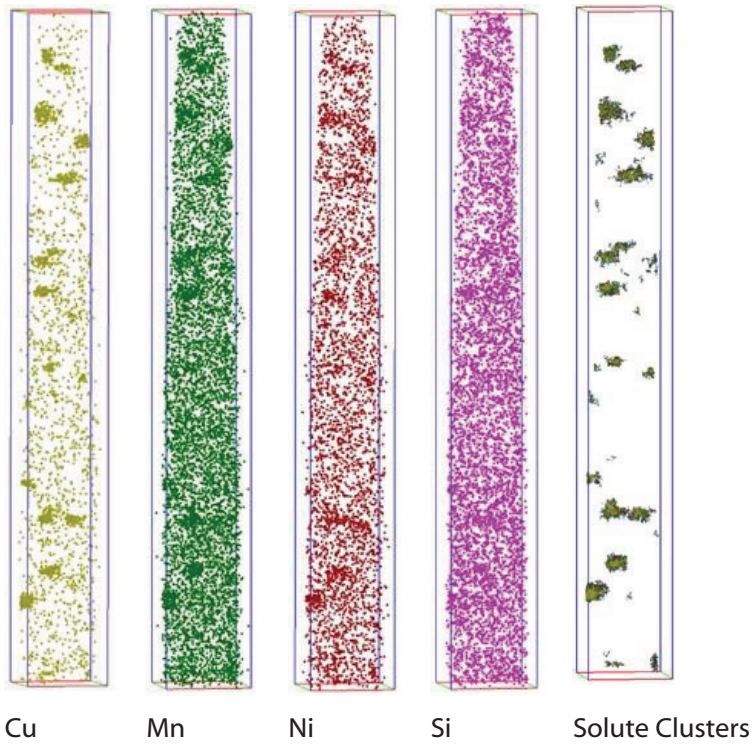

Figure 2. Distributions of Cu, Mn, Ni and Si atoms and identification of solute clusters in WV388. Extents of outline box 14x14x105nm^3.

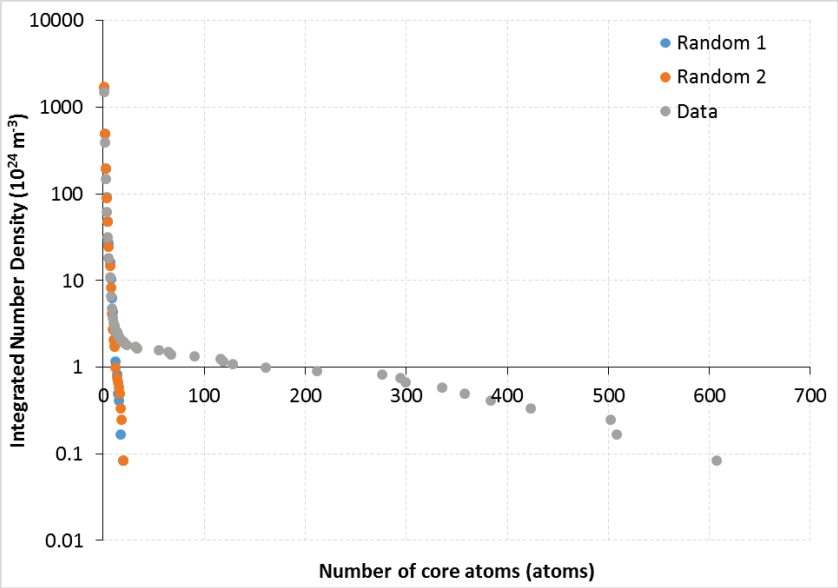

Figure 3. Integrated number density of clusters versus number of core atoms for WV388 and randomised WV388.

Data from all the analyses are summarised in Table 3. Unsurprisingly the Ni content of the clusters is strongly dependent on the bulk Ni. Similarly, for both the high and low Ni welds, the observed Cu content in the clusters increases with increasing bulk Cu content. A comparison between SH533 (low Ni, high dose) and WV388 or WV013 (high Ni, high dose) shows that the extent of precipitation in terms of cluster volume fraction and number density increases with increasing bulk Ni.

The extent of precipitation in SL092 was very low, which is consistent with expectations from a low Cu, low Ni weld. Only a few solute clusters were observed and so the mean cluster composition should be treated with caution. In the other samples examined, there is some evidence for higher Mn concentrations in the clusters formed in the high Ni welds when compared with the low Ni welds.

Table 3. Summary of characteristics of irradiation-induced solute clusters observed by APT. Cluster data are averages from several experiments.

Sample	Bulk Cu (at.%)	T_{irr} (°C)	Dose (mdpa)	ΔHv	Cluster composition (at.%)					Volume fraction of clusters (%)	Number density (10^{24} m^{-3})	Mean diameter (nm)
					Cu	Mn	Ni	Si	Fe			
SL 092	0.1	290	32	26	23.0	16.2	6.5	6.2	48.2	0.1	0.3	2.3
SH 061	0.45	255	8.3	54	29.8	9.4	5.9	2.6	52.3	0.5	1.8	1.9
SH 511*	0.52	310	8.7	44	39.5	8.2	4.7	1.7	45.5	0.3	0.6	2.3
SH 553	0.52	255	16	67	36.9	10.8	4.8	3.3	43.9	0.4	2.3	1.9
2W2.220	0.2	225	16	62	5.1	13.0	22.4	10.4	49.0	0.4	5.9	1.4
2W2.276	0.2	310	12	35	6.9	11.2	21.3	7.3	52.7	0.7	3.8	1.6
WV 013	0.55	225	24.4	99	9.3	10.7	20.6	8.2	51.0	1.0	9.2	1.5
WV 388	0.55	310	17.4	89	11.7	10.4	17.2	4.9	54.7	2.0	3.9	2.4

*A large Cu PWHT precipitate was observed in the data obtained from SH511. This region was excluded from the analysis to ensure only irradiation induced solute clusters were characterised.

DISCUSSION

In this section the relationships between the irradiation variables (dose and irradiation temperature), observed clustering of solute atoms and change in mechanical properties are explored.

Increase in Hardness as a Function of Dose

Figure 4 shows the change in hardness as a function of the square root of the neutron dose. Irradiations at lower temperatures result in higher hardening for a given dose and material. The data are consistent with a linear or near linear trend for each of the individual materials.

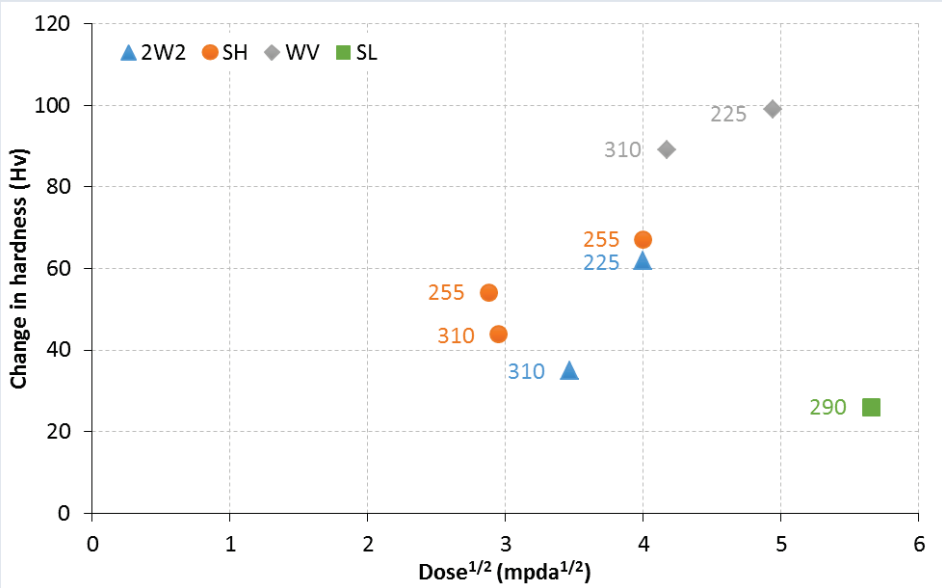

Figure 4. Change in hardness versus square root of the neutron dose received for samples studied in this report.

Increase in Cluster Volume Fraction as a Function of Dose

Figure 5 shows the volume fractions of clusters versus the neutron dose. Clear trends with material or irradiation temperature are difficult to identify. However, it appears that in the WV steels, higher temperature results in a higher volume fraction of clusters. This is less clear for the other materials, and it is possible that the opposite effect is seen in the SH material. These observations may not be inconsistent. At higher temperatures cluster growth can occur, as Odette et al. found when analysing data from the IVAR programme [15]. Monte Carlo simulations, albeit in pure Fe and model alloys, predict that at lower temperatures both the number density of self-interstitial ions and vacancy clusters will increase [2,20]. In welds, solute atoms will be associated with some of these matrix features (which are more prevalent at lower irradiation temperatures) and hence may be detected as clusters in APT using the maximum separation method. The relative importance of these two mechanisms may well depend on the Ni content of the weld.

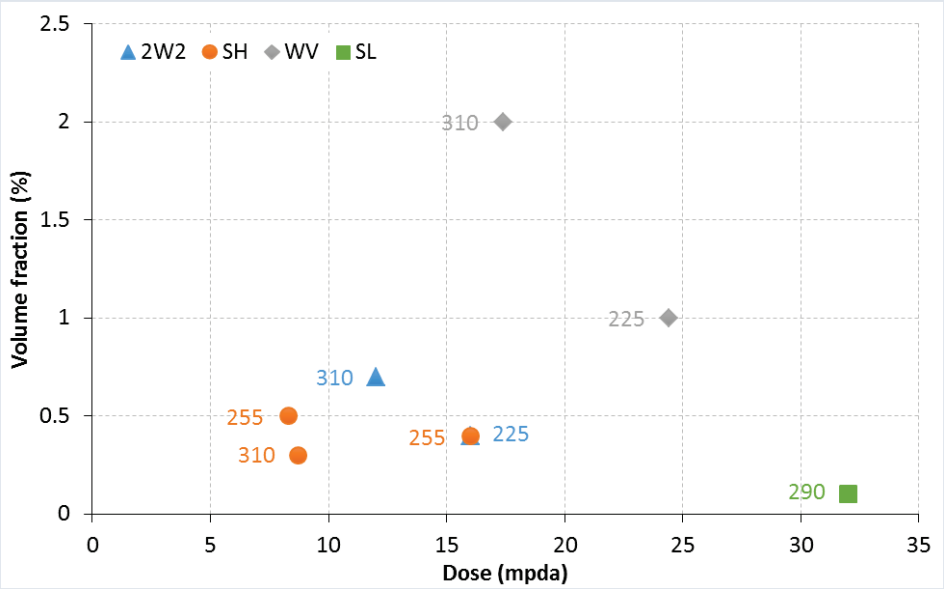

Figure 5. Volume fraction of clusters as a function of neutron dose.

Increase in Hardness as a function of Cluster Volume Fraction

The change in hardness versus the square root of the volume fraction is given in Figure 6. From the Russell Brown model [4] a linear relationship is expected (if the hardening features are the same size). There is a general trend of increasing hardness with cluster volume fraction, although the data are somewhat scattered. Some scatter is expected given the relatively small volumes of material being analysed and the fact that microstructural features other than solute clustering are also present and which contribute to hardening. Indeed, the total hardening will result from both irradiation-induced solute clusters and matrix damage. The contribution from matrix damage is likely to be greater at lower irradiation temperatures. Thus, as seen in Figure 6, the observed hardness at a given volume fraction of solute clusters tends to be higher at lower irradiation temperatures. This is consistent with the fact that Figure 4 suggests that there is potentially higher hardening at lower temperature (for a given dose).

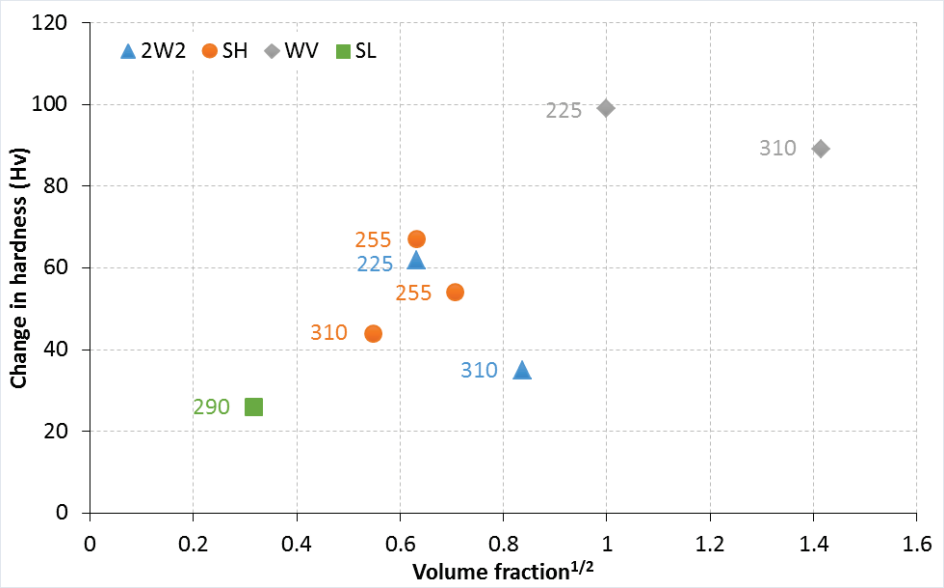

Figure 6. Change in hardness as a function of the square root of the volume fraction of clusters.

Effect of Irradiation Temperature

The discussion has already highlighted a complex relationship between irradiation temperatures and irradiation damage. The contribution from matrix damage to the mechanical property response will be greater at irradiation temperatures but only a fraction of these features will be identified by APT. The atom probe is not sensitive to vacancies and has insufficient resolution to identify whether individual atoms are interstitials or reside on lattice sites. At higher irradiation temperatures the increasing size of solute clusters is consistent with cluster growth as also observed by Odette et al. For instance, the clusters observed in 2W2.220 (T_{irr}=225°C, 16mdpa) were smaller than those observed in 2W2.276 (T_{irr}=310°C, 12mdpa). Similarly the clusters observed in WV013 (T_{irr}=255°C, 24.4 mdpa) were smaller than those observed in WV388 (T_{irr}=310°C, 17.4mdpa).

In addition there are subtleties associated with compositions of the irradiation-induced features as summarised in Table 4. Specifically, their Si content is higher at lower irradiation temperatures.

Table 4. Observed Si content of irradiation-induced clusters as a function of material and irradiation temperature.

Material	225°C Irradiation	310°C Irradiation
2W2	~10%	~7%
SH	~3%	~2%
WV	~8%	~5%

CONCLUSIONS

APT has been performed on eight RPV test welds irradiated at a range of temperatures between 225°C and 310°C. Atom maps were used to visually identify the presence of irradiation-induced clusters containing solute atoms and then the maximum separation method applied to characterise the extent of solute precipitation in terms of solute cluster size, composition and number density. A number of conclusions can be drawn

- Where multiple examinations have been made on a particular material condition, the results are reasonably self-consistent. In particular similar cluster sizes and compositions were observed.
- As the Cu content is reduced, the driving force for clustering decreases. Thus precipitation in SL092 (0.1%Cu, 32mpda) was very much lower than observed in SH (~0.5%Cu, lower dose).
- For both the low and high Ni steels, the higher the bulk Cu content the higher the observed Cu composition of the clusters.
- At lower irradiation temperatures, the clusters appear to contain more Si.
- In general smaller clusters were observed in the high Ni steels. The exception was the high Ni weld WV388 in which relatively large irradiation induced clusters were observed due to the high irradiation temperature.
- At higher irradiation temperatures the clusters are more developed due to thermal growth.
- There is a general trend of increasing hardness with cluster volume fraction, and for an increasing contribution from matrix damage to the irradiation hardening response at lower irradiation temperatures.

REFERENCES

[1] C.A. English and J.M. Hyde, 'Radiation Damage of Reactor Pressure Vessel Steels", Comprehensive Nuclear Material, Elsevier, Ed. R. Konings, 2012, ISBN: 9780080560274.
[2] N. Soneda, “Irradiation Embrittlement of Reactor Pressure Vessels (RPVs) in Nuclear Power Plants“, Woodhead Publishing Series in Energy: Number 26, 2014 ISBN978-1-84569-967-3

[3] Barton, P.J., Harries, D.R. and Mogford, I.L., "Effects of Neutron Dose Rate and Irradiation Temperature on Hardening", J. Iron Steel Inst. (London), vol. 203, 1965, pp 507-510
[4] Grounes M., "Review of Swedish Work on Irradiation Effects in Pressure Vessel Steels and on Significance of Data Obtained", *Effects of Radiation on Structural Metals, ASTM STP 426*, American Society for Testing and Materials, Philadelphia, 1967, pp 224-259; early considerations summarised in *Steels for Reactor Pressure Circuits*, Report of a Symposium held in London 30 November - 2 December, 1960, Iron and Steel Institute, London, 1961, pp 422-426.
[5] Jones, R.B., and Williams T. J., "The Dependence Of Radiation Hardening And Embrittlement On Irradiation Temperature" *Effects of Radiation on Materials:17th International Symposium, ASTM* 1270, Eds D.S. Gelles, R.K. Nanstead, A.S. Kumar, and E.A.Little, ASTM 1996, 569
[6] M.A. Sokolov and R.K. Nanstad, Comparison of Irradiation-Induced Shifts of KJc and Charpy Impact Toughness for Reactor Pressure Vessel Steels, in Effects of Radiation on Materials: 18th Int. Symp., ASTM STP 1325 (1999), p167-189
[7] Hawthorne et al. "Exploratory Studies of the Effects of Irradiation Temperature on Mechanical Properties of Structural Steels and Welds", Effects of Radiation on Materials: 16th Int. Symp, ASTM STP 1175, 1993, p306-331
[8] Haggag, F. M., 16th International Symposium On Effects Of Radiation On Materials: ASTM STP 1175, (1993) p.172.
[9] Wire, G. L., Beggs, W. J. AND Leax, T. R., "evaluation Of Irradiation Embrittlement Of A508 Gr4N And Comparison To Other Low-Alloy Steels" *Effects of Radiation on Materials: 21st Int. Symp., ASTM STP 1447*. Eds. Grossbeck et al, pub ASTM International, West Conshohocken, USA (2004) pp. 179-193
[10] Williams, T. J., Ellis, D., Swan, D. I., McGuire, J., Walley, S. P., English, C. A., Venables, J. H., and Ray, P. H. N., "The Influence Of Copper, Nickel And Irradiation Temperature On The Irradiation Shift Of Low Alloy Steels", *Proc of 2nd International Symposium on Environmental Degradation of Materials in Nuclear Power Systems - Water Reactors*, held September 1985, pub. ANS 1986.
[11] J.M. Hyde and C.A. English, "Microstructural Characterisation Techniques for Mechanistic Understanding of Irradiation Damage", in "Irradiation Embrittlement of Reactor Pressure Vessels (RPVs) in Nuclear Power Plants", Woodhead Publishing Series in Energy: Number 26, 2014 (pp. 211-294) ISBN978-1-84569-967-3
[12] E. Meslin, A. Barbu, L. Boulanger, B. Radiguet, P. Pareige, K. Arakawa and C. C. Fu, "Cluster-Dynamics Modelling Of Defects In a-Iron Under Cascade Damage Conditions" J. Nuclear Mater., in press 2008.
[13] H. Watanabe, Masaki, S., Masubuchi, S., Yoshida, N. and Dohi, K., "Effects Of Mn Addition On Dislocation Loop Formation In A533B And Model Alloys" J. Nuclear Mater., 439 (2013) 268-275.
[14] R.B. Jones, and C.J.Bolton, , "Neutron Radiation Embrittlement Studies In Support Of Continued Operation And Validation Of Sampling Of Magnox Reactor Steel Pressure Vessels And Components", 24th Water Reactor Safety Meeting 21-23 October 1996
[15] E.D. Eason , G.R. Odette , R.K. Nanstad , T. Yamamoto and M.T. EricksonKirk, *A physically based correlation of irradiation-induced transition temperature shifts for RPV steels* , ORNL/TM-2006/530 , Oak Ridge National Laboratory, Oak Ridge, TN , 2007
[16] D. Blavette, B. Deconihout, A. Bostel, J. M. Sarrau, M. Bouet and A. Menand, The tomographic atom probe: A quantitative three dimensional nanoanalytical instrument on an atomic scale, Review of Scientific Instruments 64, 2911 (1993); doi: 10.1063/1.1144382
[17] J.M. Hyde, M.G. Burke, B. Gault, D.W. Saxey, P. Styman, K.B. Wilford, T.J. Williams, Atom probe tomography of reactor pressure vessel steels: An analysis of data integrity, *Ultramicroscopy* 111, 676-682, 2011.
[18] J.M. Hyde and C.A. English, 'An Analysis of the Structure of Irradiation induced Cu-enriched Clusters in Low and High Nickel Welds', Invited paper in symposium R 'Microstructural processes in irradiated materials', Fall MRS November 2000, R6.6
[19] J.M. Hyde, E.A. Marquis, K.B. Wilford, T.J. Williams, A sensitivity analysis of the maximum separation method for the characterisation of solute clusters, *Ultramicroscopy* 111, 440-447, 2011.
[20] Domain, C. Becquart, C. S. and Malerba, L. "Simulation Of Radiation Damage In Fe Alloys: An Object Kinetic Monte Carlo Approach" J. Nuclear Mater., 335 (2004) 121-145.